Supplement of Atmos. Chem. Phys., 20, 4607–4635, 2020
https://doi.org/10.5194/acp-20-4607-2020-supplement

Atmospheric Chemistry and Physics
Open Access
EGU

Supplement of

Characterization of organic aerosol across the global remote troposphere: a comparison of ATom measurements and global chemistry models

Alma Hodzic et al.

Correspondence to: Alma Hodzic (alma@ucar.edu)

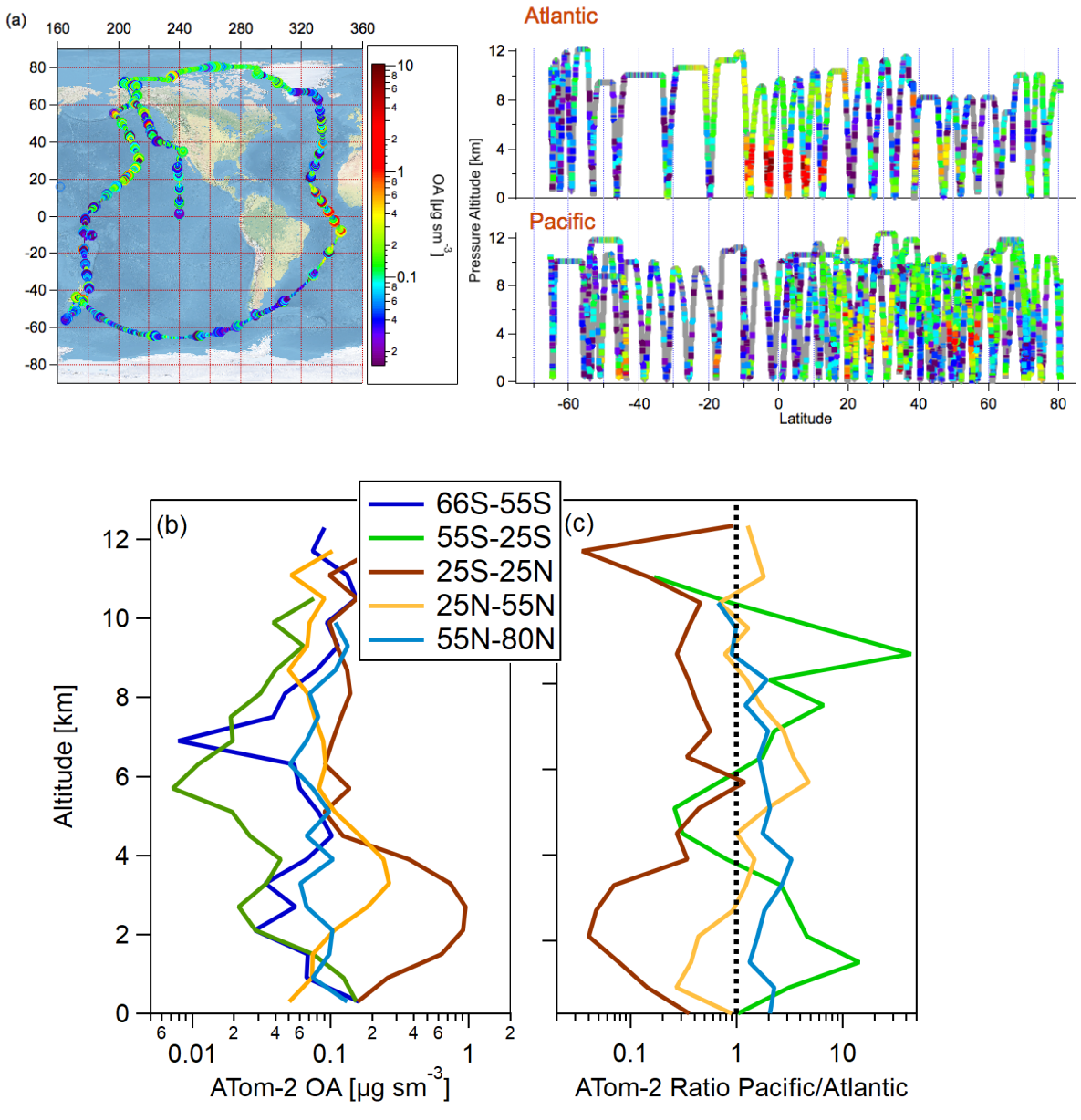

Figure S1: (Upper plots) Vertical distribution of organic aerosol concentrations (OA, µg sm^{-3}) along the ATom-2 flight tracks that took place during February 2017. (Lower plots) The corresponding average OA vertical profiles for each latitude region, and ratios between Pacific and Atlantic OA concentrations in each latitude region.

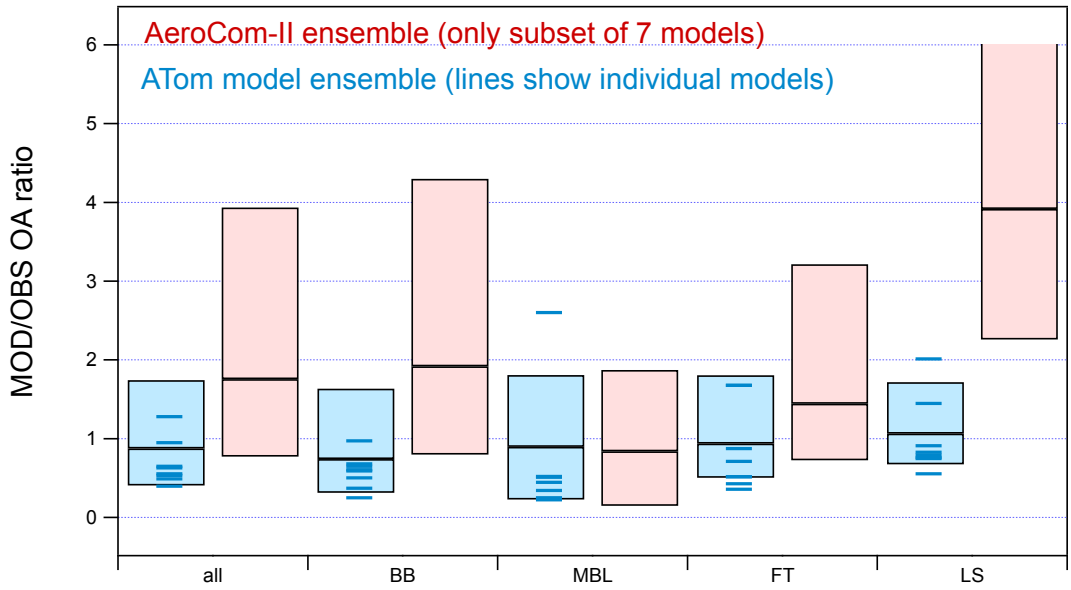

Figure S2: Similar to figure 3, showing the ratios between predicted and observed OA concentrations for all ATom-1 flights as calculated for the ATom model assemble and a subset of AeroCom-II models in different regions. The AeroCom-II subset of models incudes CAM5-MAM3, CCSM4-hem, ECHAM5-HAM2, GEOSChem-APM 8.2, GEOSChem 9, GISS-TOMAS and GMI (see Tsigaridis et al., 2014 for their description).

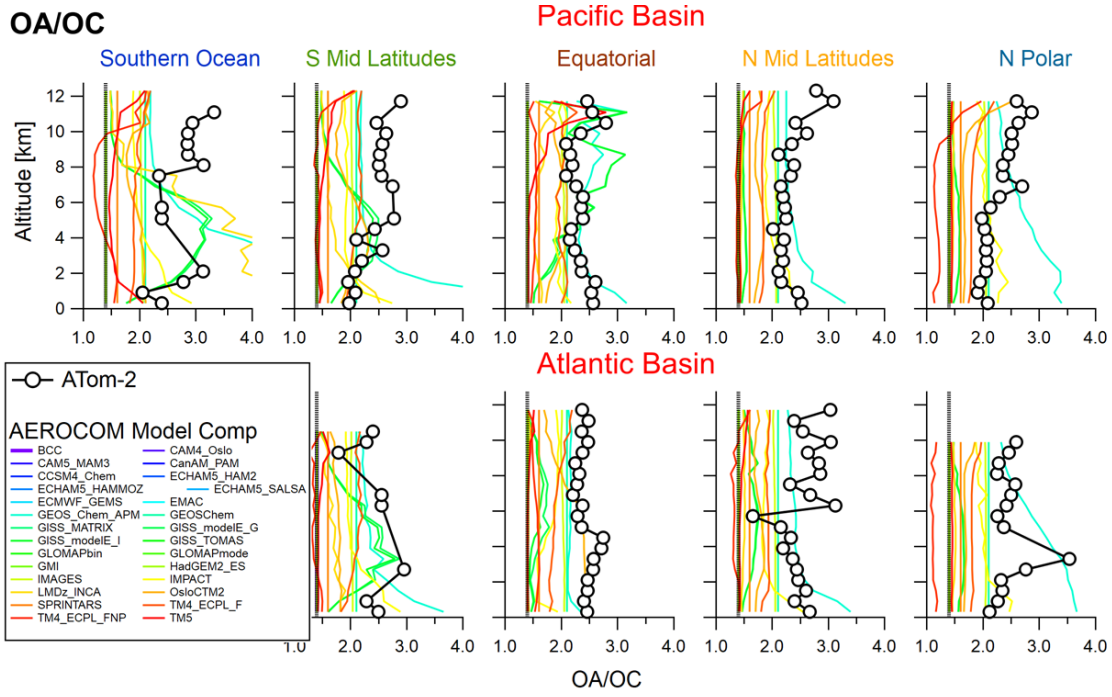

Figure S3: Vertical profiles of OA / OC ratios as measured during the ATom-2 deployment and as calculated in the AeroCom-II models.

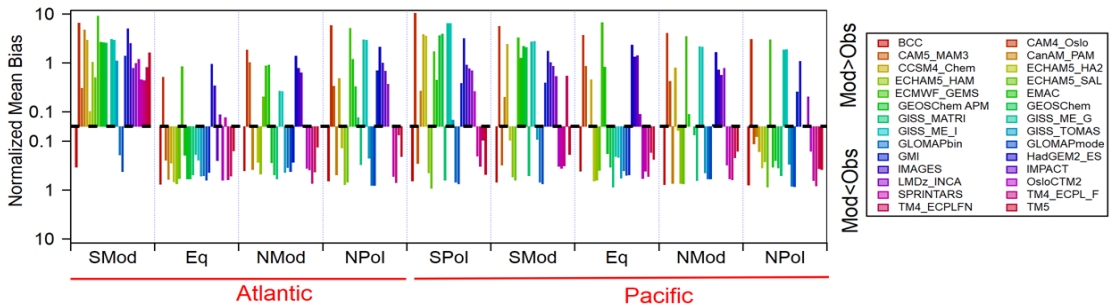

Figure S4: Quantitative comparison of OA measured during ATom-1 (upper panel) and ATom-2 (lower panel) deployments with the average predictions of the AeroCom-II models. The normalized mean bias is shown for all individual model simulations for various latitudinal regions and for both the Atlantic and Pacific basins.

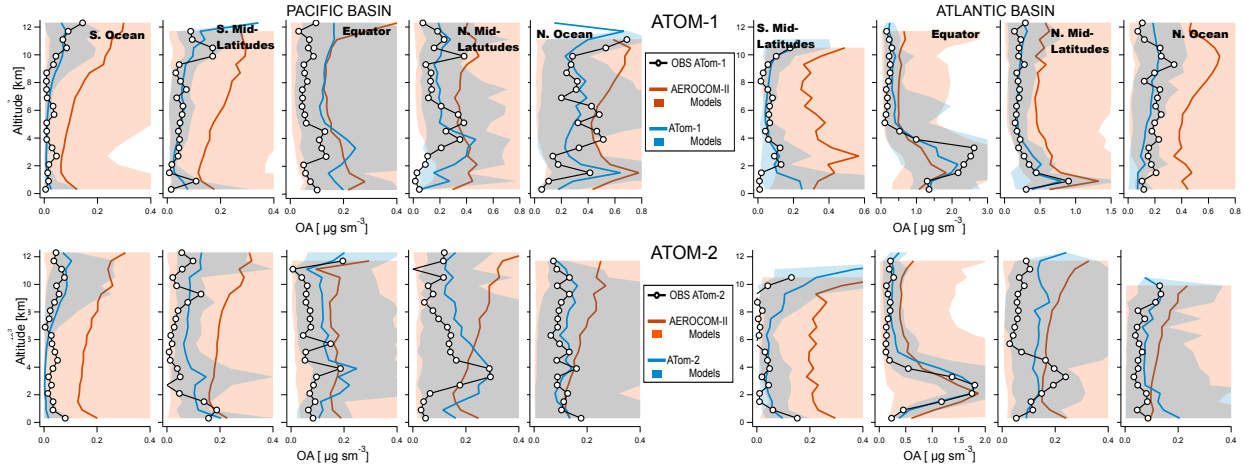

Figure S5: Similar to figure 4 but on a linear scale.

a)

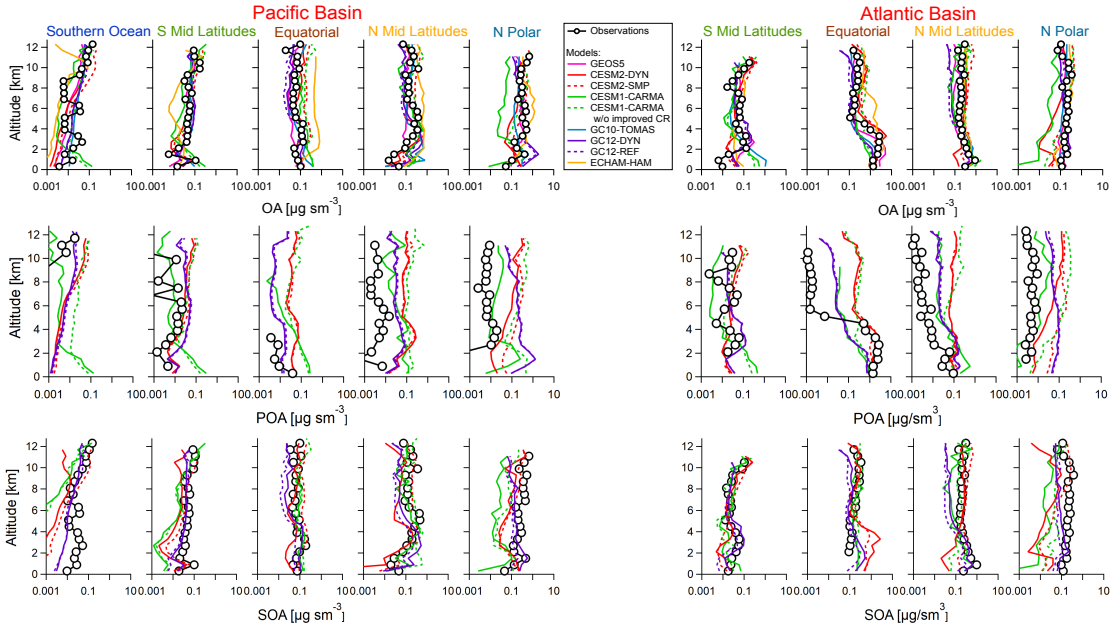

b)

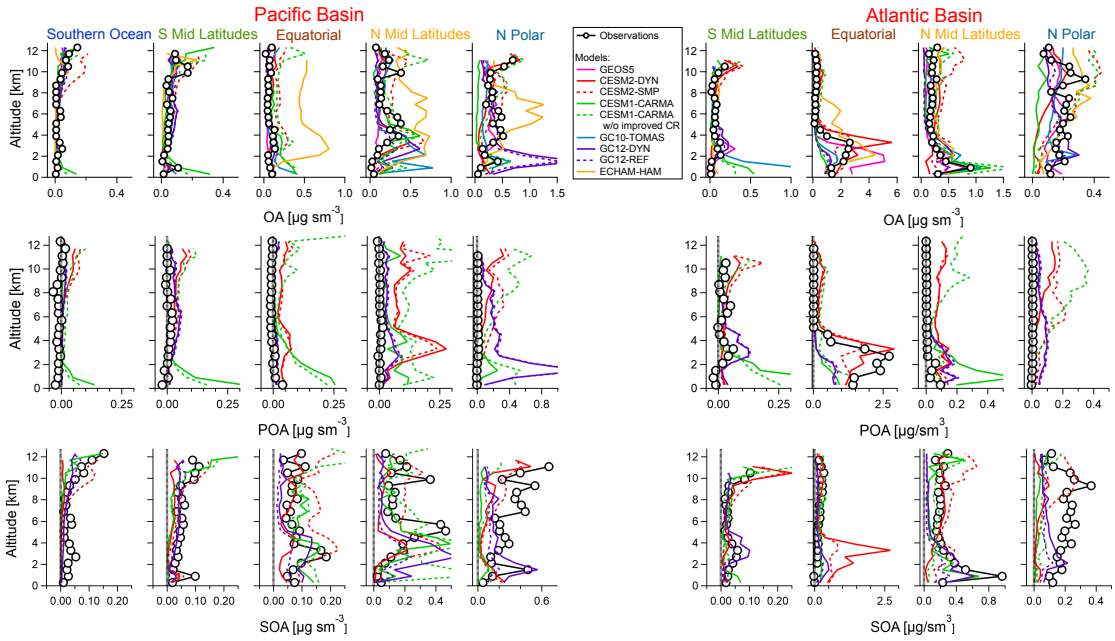

Figure S6: Comparison of latitude-averaged predicted OA, POA and SOA vertical profiles with ATom-1 measurements taken over the Pacific (left side) and the Atlantic basins (right side) for all current model simulations shown on a logarithmic (a) and linear (b) scales.

a)

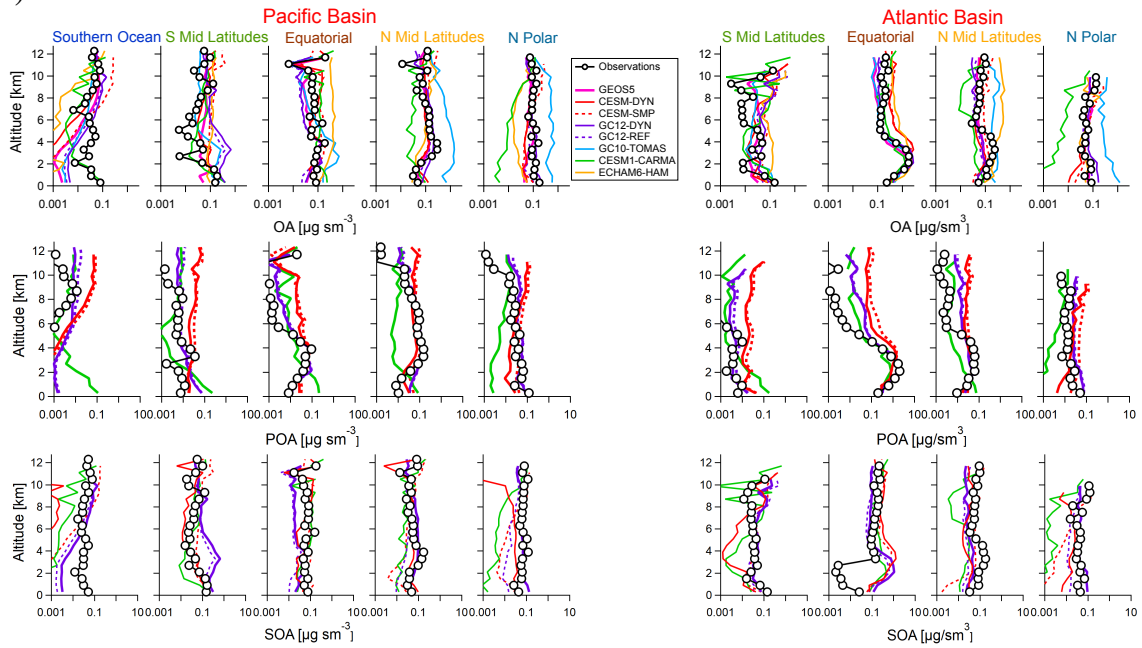

b)

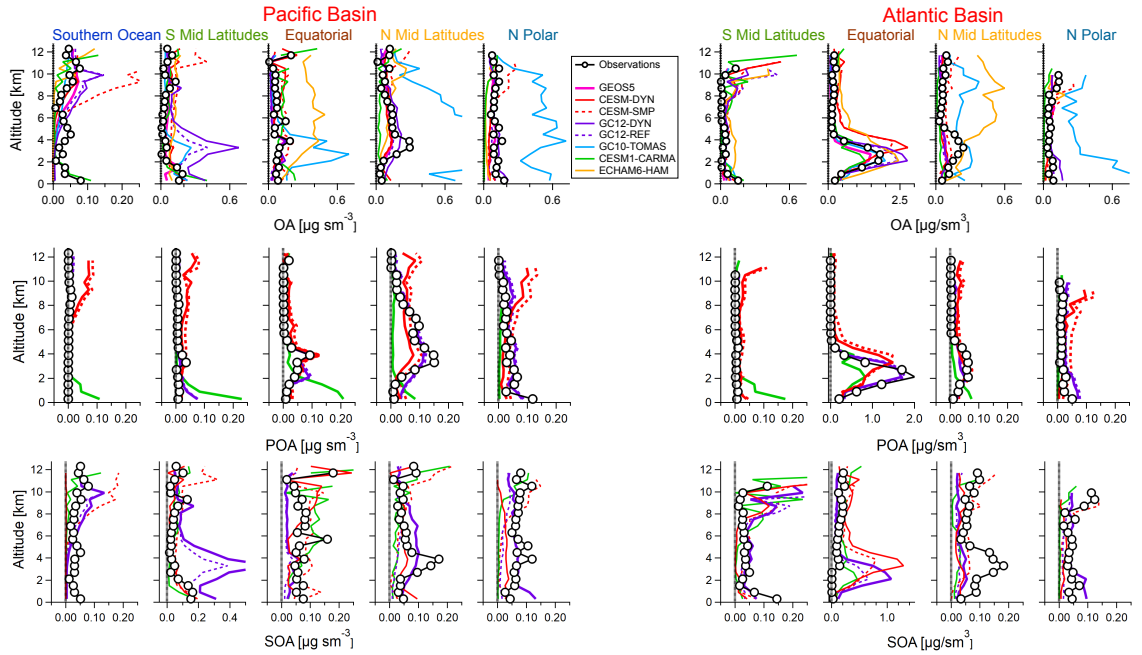

Figure S7: As Figure S6 for ATom-2 shown both on a logarithmic (a) and linear (b) scales.

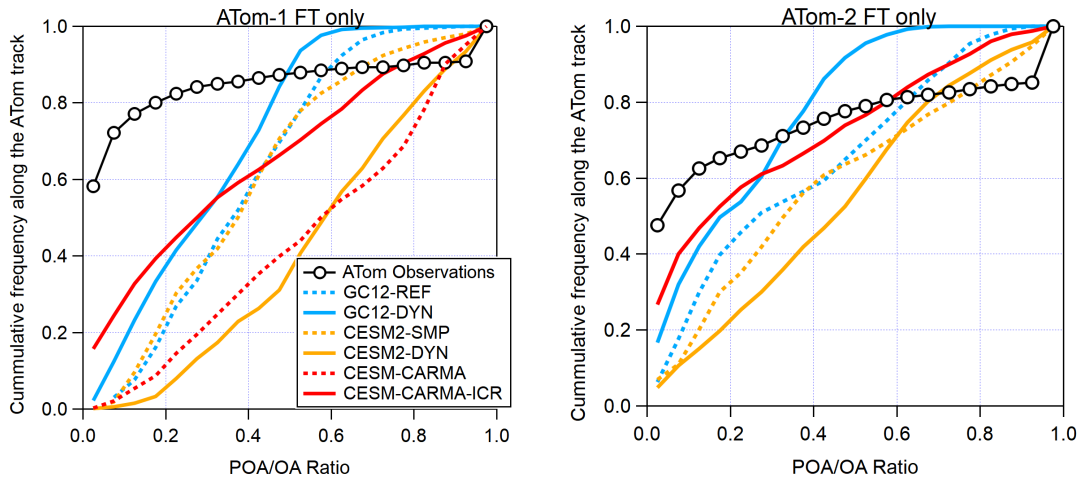

Figure S8: POA/OA distributions (free troposphere only) from Figure 7 shown as cumulative distributions (CDF). Note that for the OA/BC ratios observed for ATom specifically, the green curves in Fig S9b and S9d (BB_{ratio}=2) are closer to the real distribution.

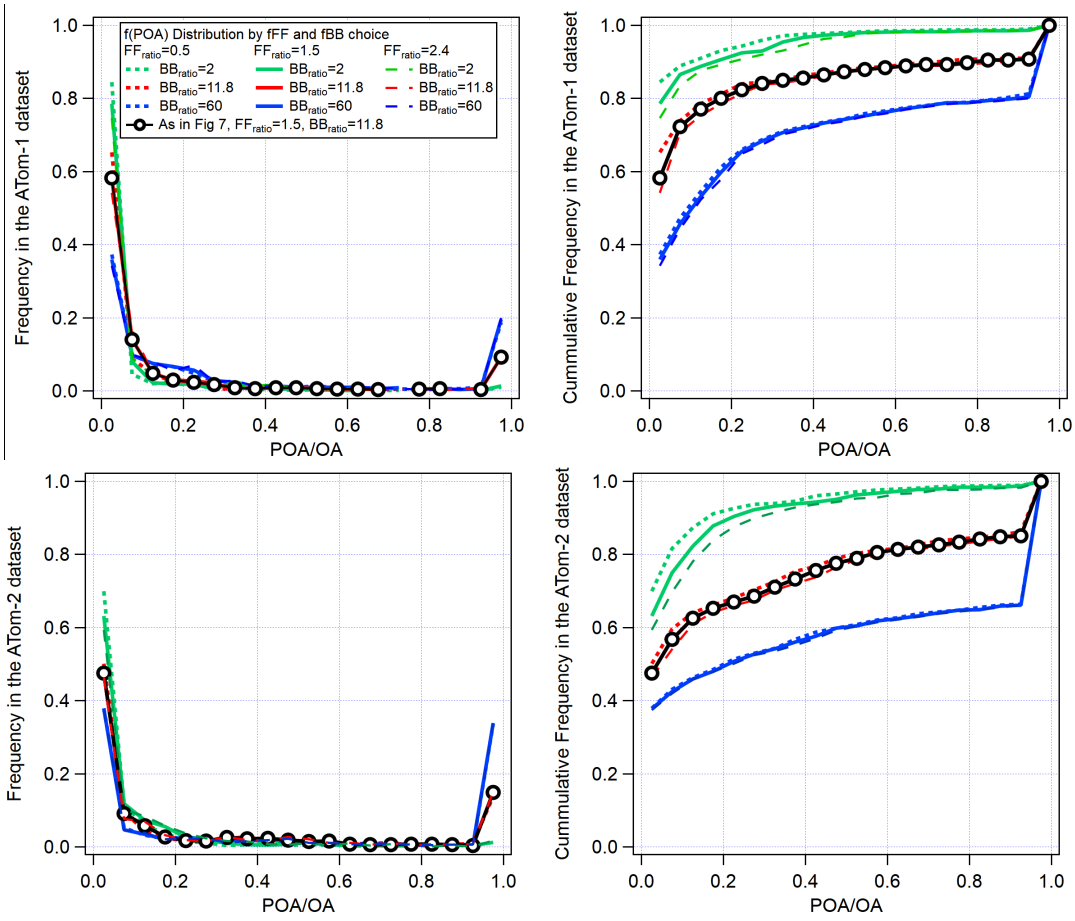

Figure S9: Sensitivity of the overall measured POA/OA distribution to different estimates of POA/BC ratios for both urban and BB sources covering the range of values shown in Table S1 and S2, both for the frequency and cumulative frequency distribution (left/right)

and ATom-1 and 2 (top/bottom). Note that for the choice of BB_{ratio} ranges, we used the range (within uncertainties) for the main global BB contributors and excluded one clear outlier, peat. This is justified since peat is a small source, mostly localized to SE Asia, and the main emissions of peat BB aerosol are outside the sampling periods of ATom-1 and 2 (Reddington et al, 2014).

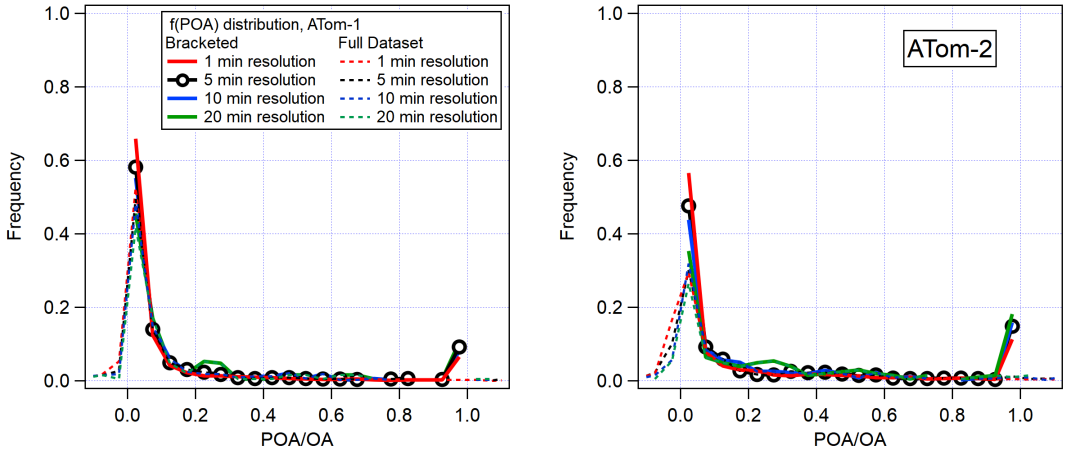

Figure S10: Exploring the impact of OA data below detection limit (DL) by increasing the averaging interval on the POA/OA distributions in Figure 7 for ATom 1 and 2 (a 5 min averaging interval was used throughout the analysis discussed in Section 4.4). Also shown is the comparison of a capped (so $f_{(POA)}$=0 includes $f_{(POA)}$<0, and $f_{(POA)}$=1 includes $f_{(POA)}$>1) vs. an unconstrained histogram, for the same set of averaging intervals. In the manuscript, 5-minute averaging (capped) is used.

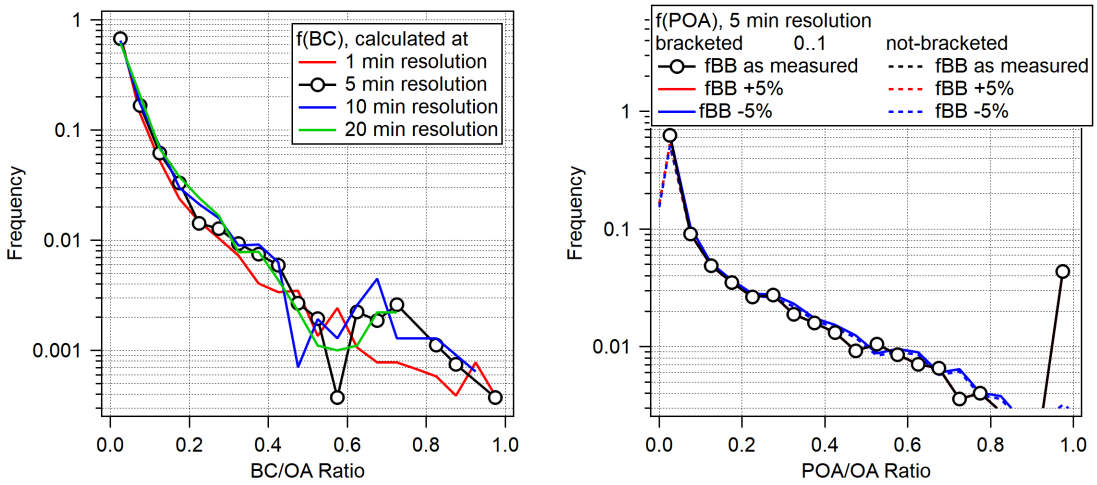

Figure S11: (left) Distribution of BC/OA ratios that are used as the basis of the estimation of $f_{(POA)}$ for all ATom deployments, shown using different averaging intervals (right) Effect of the 5% uncertainty in the f(BB) reported by the PALMS instrument on the estimation of $f_{(POA)}$, using both bracketed and not bracketed data (cf. Figure S10).

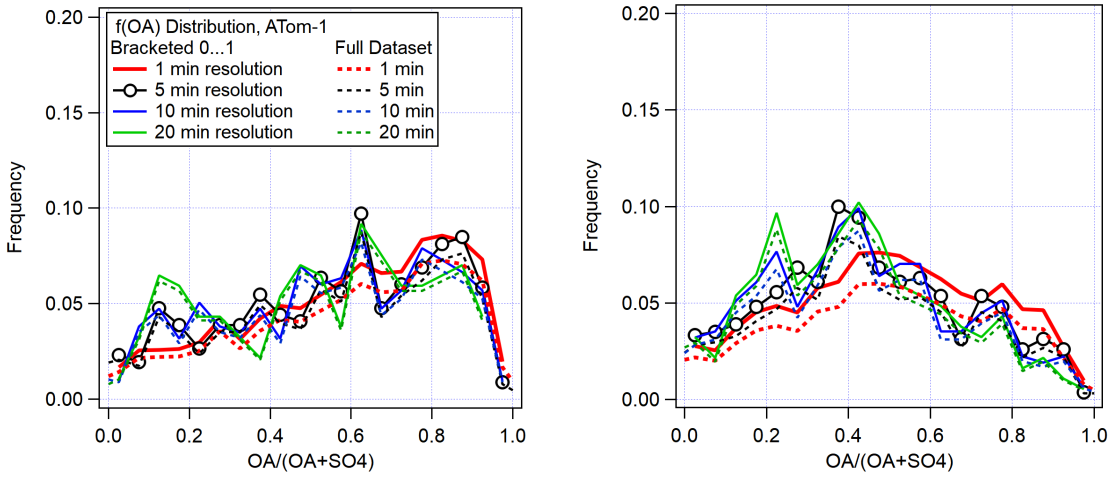

Figure S12: Exploring the impact of various data averaging frequency (from 1 to 20 minute resolutions) on the OA/(OA+SO4) distributions in Figure 9. In the manuscript, a 5-minute averaging is used. Also shown is the impact of calculating bracketed (just for ratios from 0..1) normalized frequency distributions (as used in the manuscript) vs. considering all points.

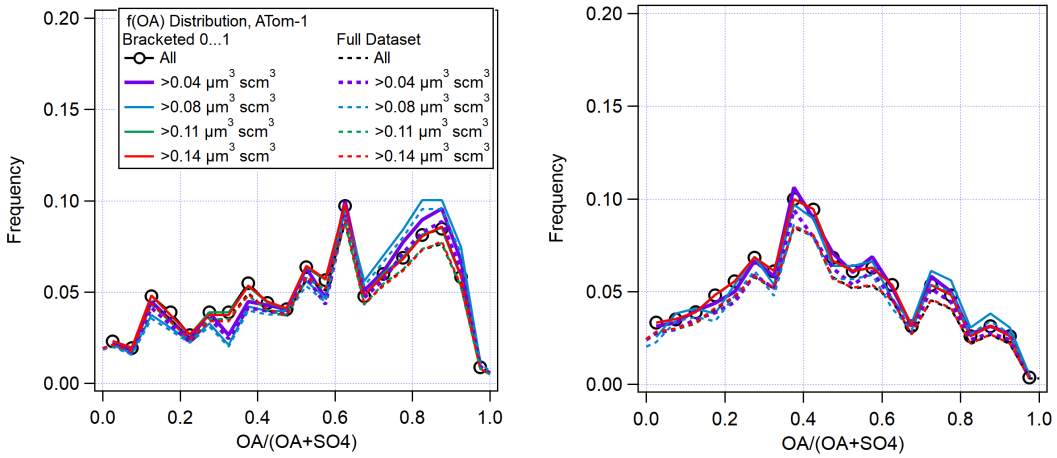

Figure S13: Exploring the impact of thresholding the 5-min averaged data by a minimum detectable aerosol volume in the PM1 range (from the NOAA SD product, see Guo et al 2019 for details) when computing the the OA/(OA+SO4) distributions in Figure 9.

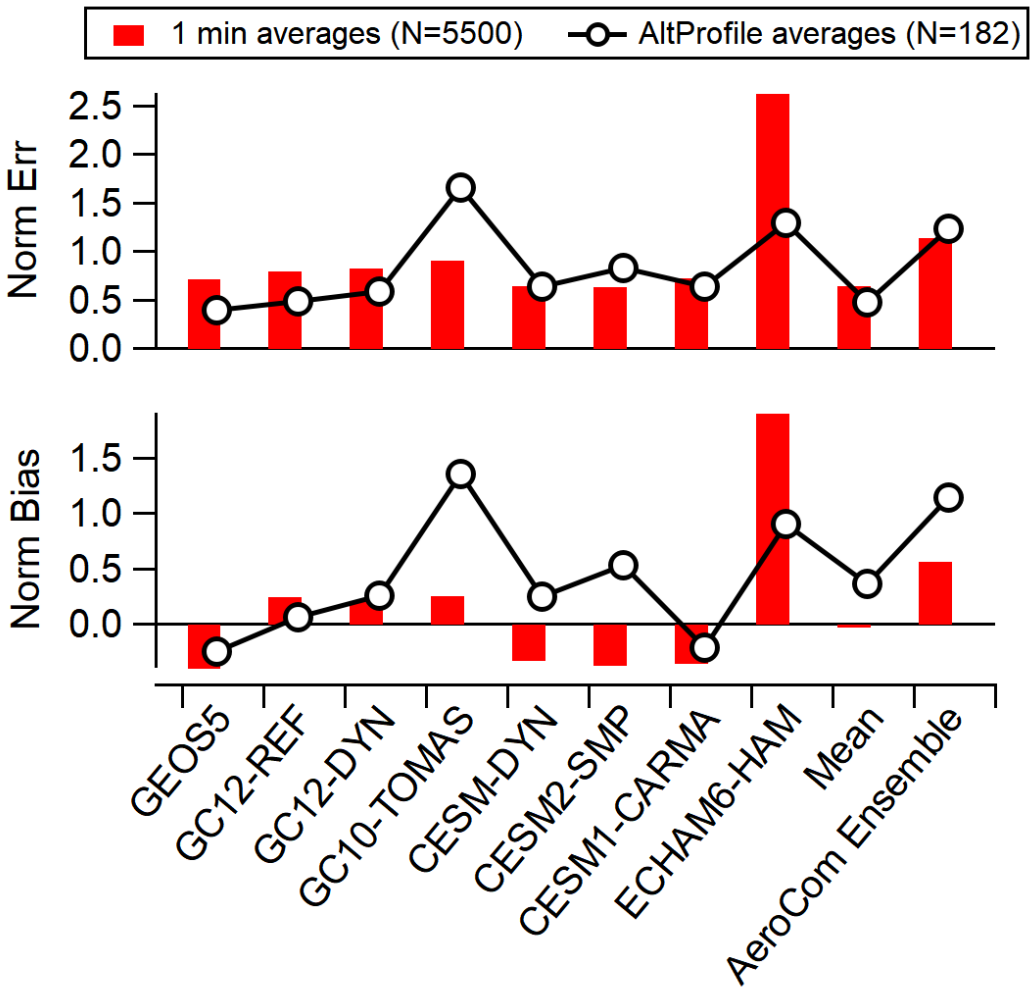

Figure S14: Normalized standard errors and biases calculated for the comparison of the measured and modeled vertical profiles (N=182, 3% of measured points under DL) and the measured and modeled flight racks at 1 min resolution as shown in Table 2 and S3 (N=5580, 32% of measured points under DL) for ATom-2.

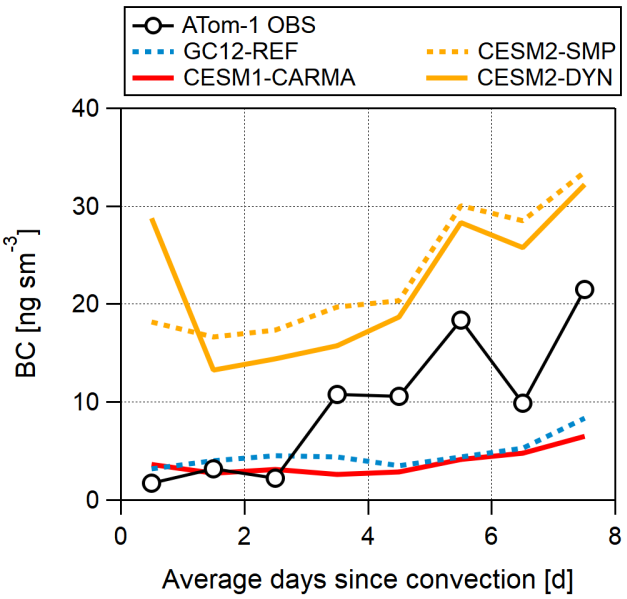

Figure S15: As Figure 8, shown for black carbon (BC).

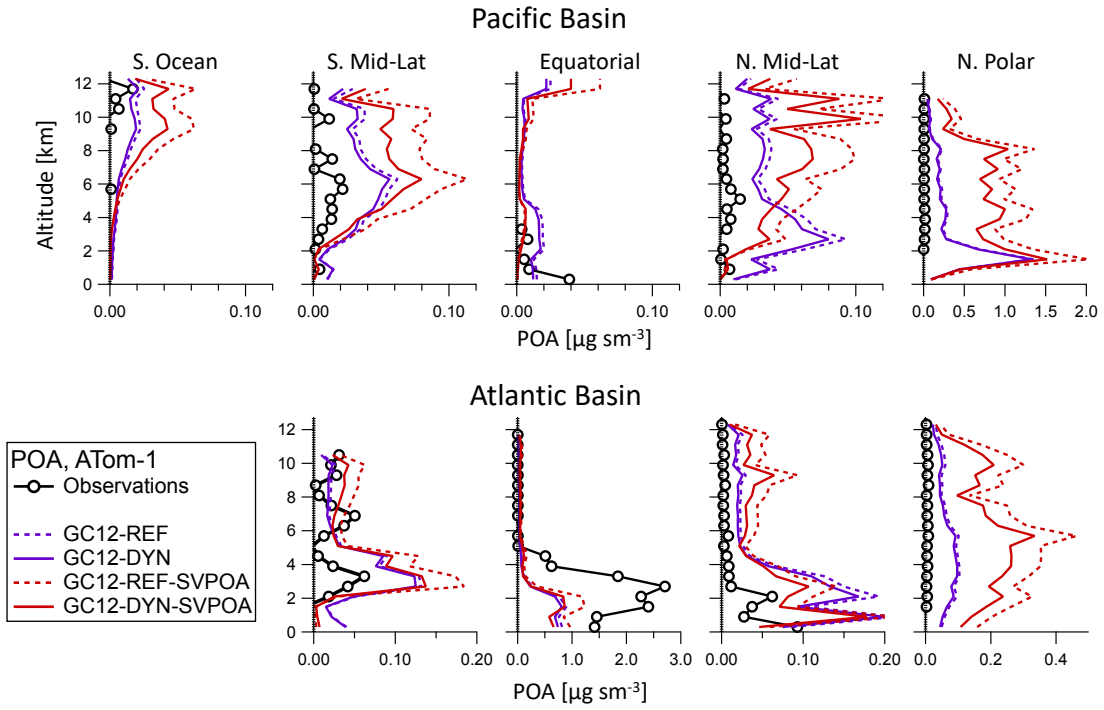

Figure S16: Sensitivity simulations to estimate the importance of the non-volatile vs. semi-volatile POA treatment in GEOS-Chem. The semi-volatile POA in GC12-REF-SVPOA (GC12-DYN-SVPOA) model configuration should be directly compared with the corresponding GC12-REF (GC12-DYN) non-volatile POA.

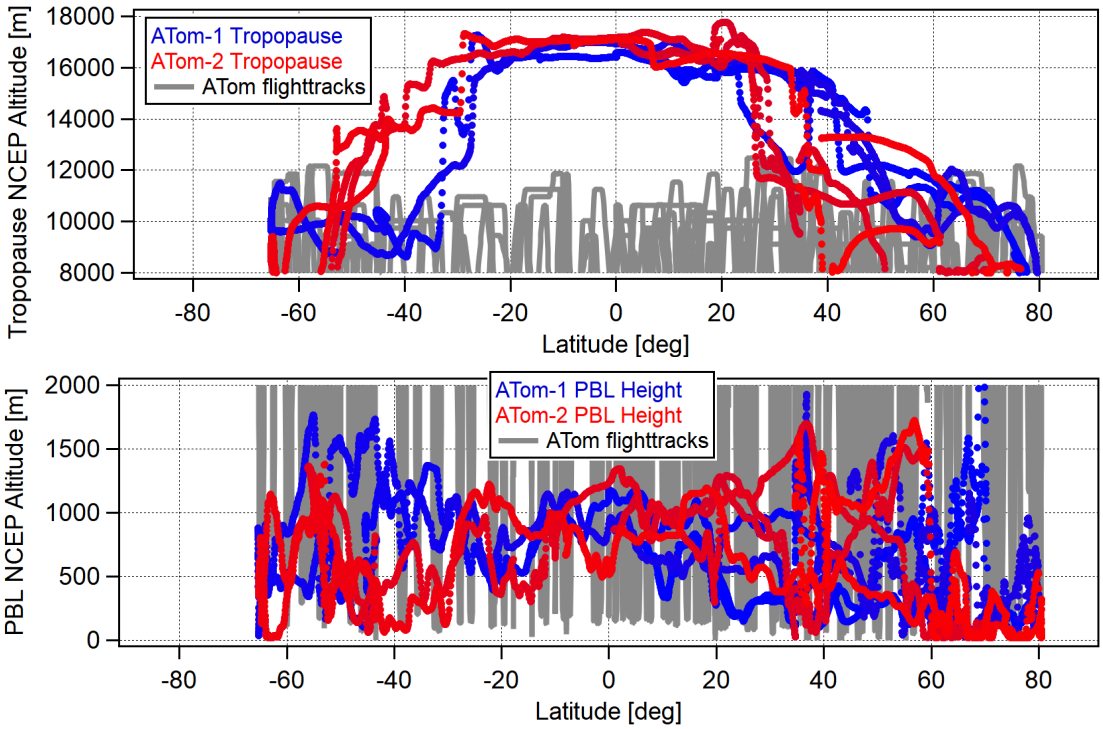

Figure S17: (top) tropopause heights from the NCEP reanalysis at each Lat/Long flown for ATom-1 (blue) and ATom-2 (green). (bottom) Planetary boundary layer (PBL) heights obtained in the same way. Values from the GEOS-5 model are very similar to these. ATom-1 and 2 flight tracks are included in grey for context.

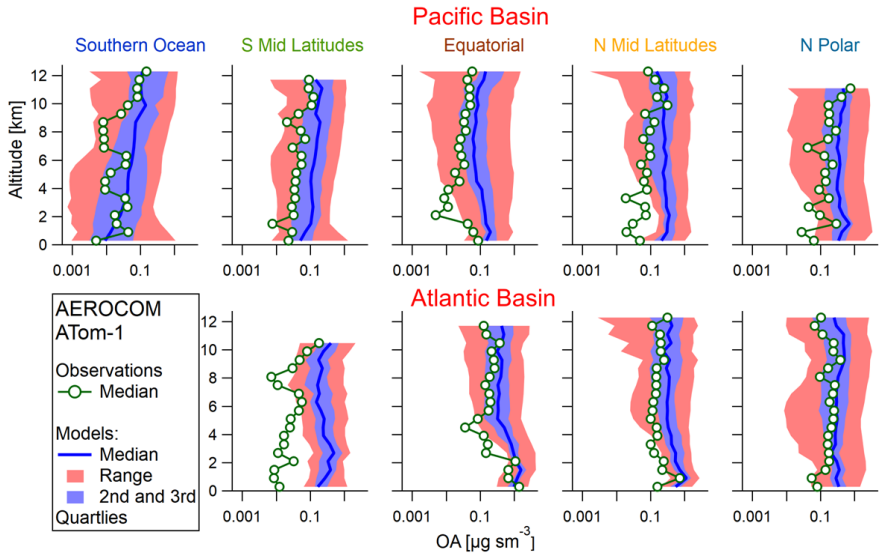

a.

b.

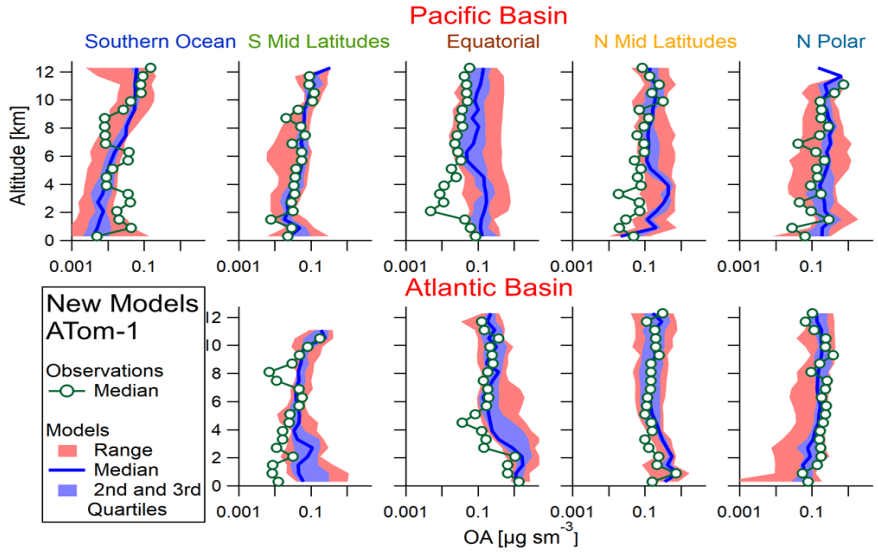
Pacific Basin
Southern Ocean
S Mid Latitudes
Equatorial
N Mid Latitudes
N Polar
Altitude [km]
0.001
0.1
Atlantic Basin
New Models
ATom-1
Observations
Median
Models
Range
Median
2nd and 3rd
Quartiles
OA [μg sm-3]

c.

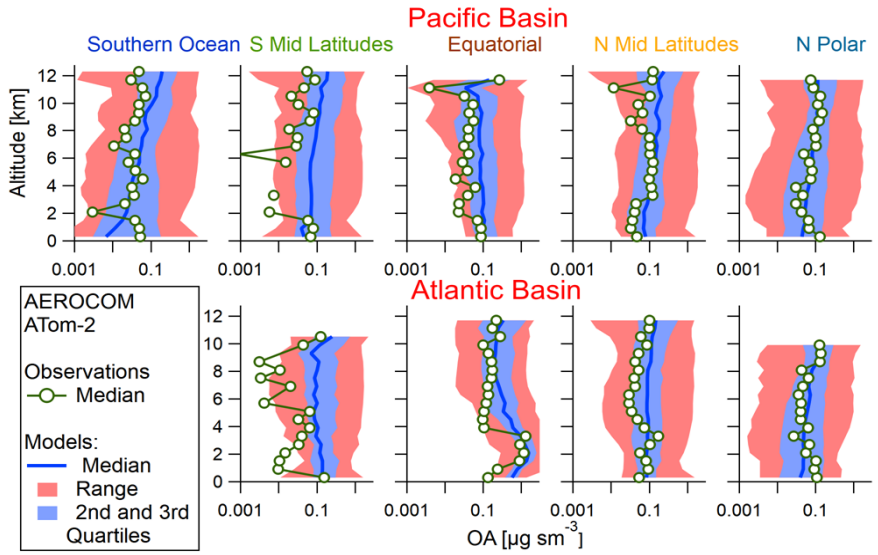
Pacific Basin
Southern Ocean
S Mid Latitudes
Equatorial
N Mid Latitudes
N Polar
Altitude [km]
0.001
0.1
Atlantic Basin
AEROCOM
ATom-2
Observations
Median
Models:
Median
Range
2nd and 3rd
Quartiles
OA [μg sm-3]

d.

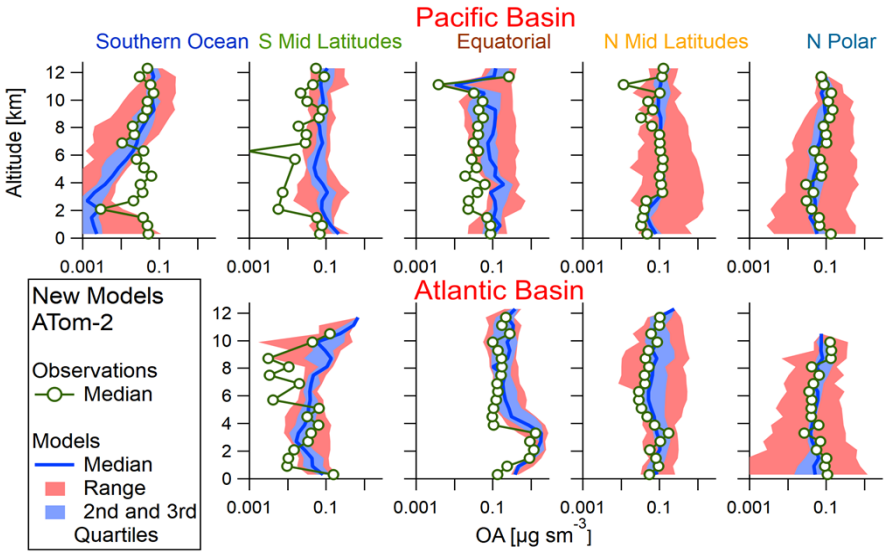
Pacific Basin
Southern Ocean
S Mid Latitudes
Equatorial
N Mid Latitudes
N Polar
Altitude [km]
0.001
0.1
Atlantic Basin
New Models
ATom-2
Observations
Median
Models
Median
Range
2nd and 3rd
Quartiles
OA [μg sm-3]

Figure S18: Comparison of OA median vertical profiles as measured during ATom-1 and predicted by the (a) AeroCom-II model ensemble and (b) ATom model ensemble. Panels (c) and (d) show the same for ATom-2, respectively (similar to figure 5 in the paper that compares OA average profiles).

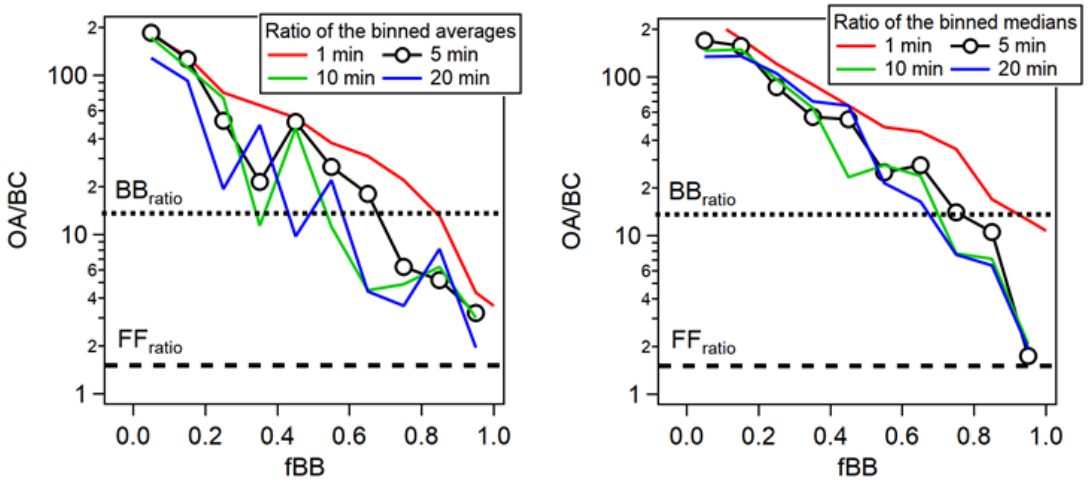

Figure S19: Distribution of the OA/BC ratio as a function of the fraction of BB influence measured by f(BB)$_{PALMS}$, calculated both as binned averages (left) and binned medians (right) for AToOm-1. Also shown are the OA/BC ratios that we currently assume based on the literature review for both anthropogenic (FF$_{ratio}$) and biomass burning sources (BB$_{ratio}$).

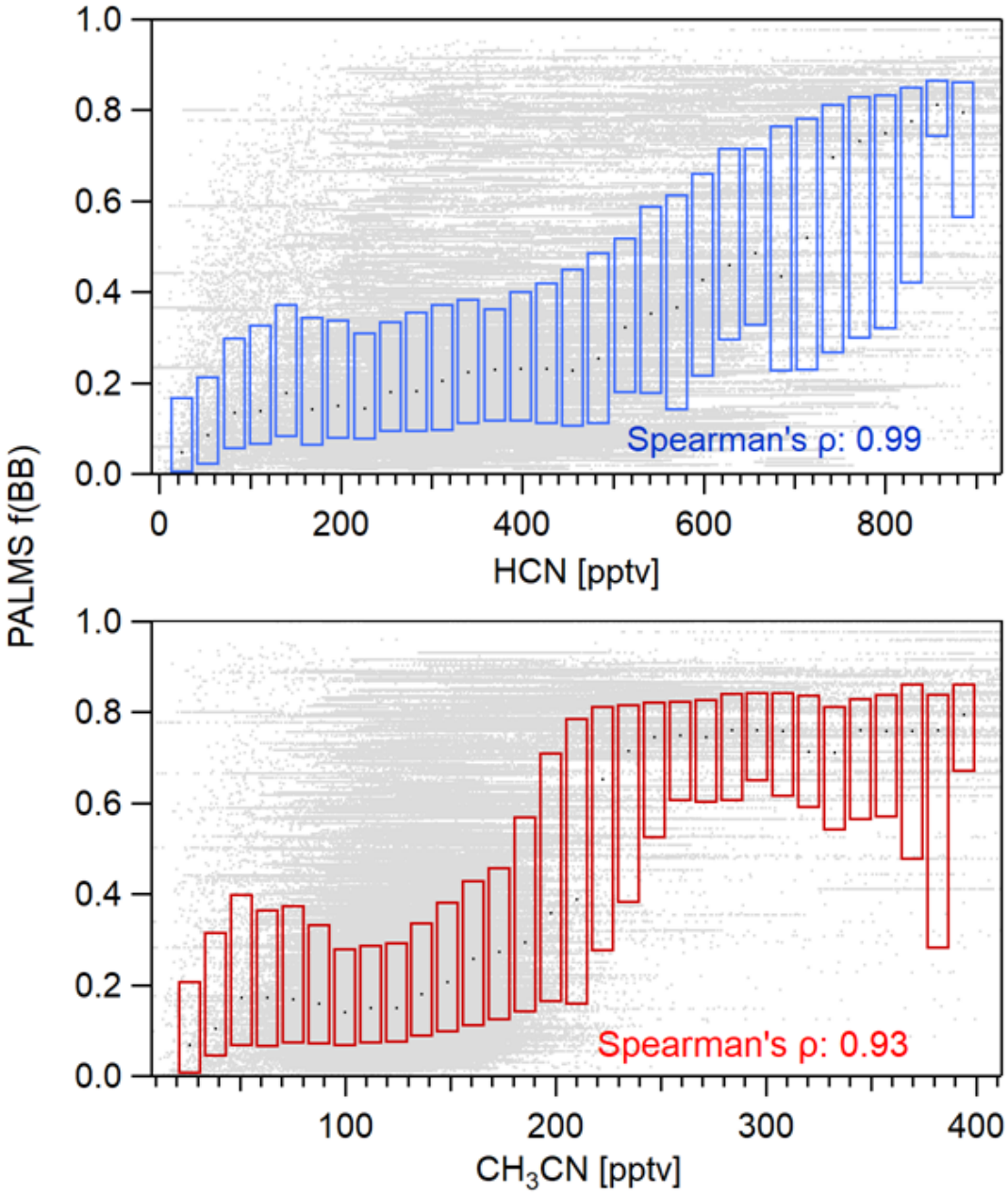

Figure S20: Correlation of f(BB) from the PALMS instrument with collocated, well characterized gas phase tracers for BB for the full ATom mission (1-4). HCN (top panel) provided by the Caltech CIMS instrument, CH_3CN (bottom panel) provided by the NCAR TOGA GC-IE instrument (Wofsy et al., 2018).

Table S1: POA/BC ratios determined in previous field and laboratory emission studies. Studies that reported well constrained urban non-BB POA based on AMS PMF determinations (highlighted in bold) were averaged to determine the value used for $(POA/BC)_{anthro}$. Studies that reported $(POA/BC)_{BB}$ are shown in italics. For the average of $(POA/BC)_{BB}$ the weighted average reported by Andreae, 2019 was used.

Source	Technique	Type of emissions	POA/BC ratio (OA measured)	POA/BC ratio (OC measured, OA/OC of 1.8 used)
Zhang et al. 2005	AMS PCA for POA EC from TOCA	Urban background	**1.41**	
Szidat et al. 2006	14C source apportionment for EC and OC	Urban mobile sources Residential burning		2.65 *11.3*
Ban-Weiss et al. 2008	OC: Filters (TOA) Aethalometer and filters for BC	Mobile sources: Light Duty Vehicles Diesel		 2.5 1.3
Aiken et al. 2009	AMS PMF for POA, SP2 for BC	Urban background	**0.8**	
Christian et al. 2010	TOT EC/OC analyzer	Cooking Stoves Trash Burning Brick Klinn Charcoal Klinn AG Burn		*6.3* *7.75* *0.27* *78* *200*
Chirico et al. 2010	AMS PMF for POA SP2 for BC	Tailpipe emissions, gas vehicle	0.16-0.3	
Minguillon et al. 2011	14C source apportionment for EC and OC, combined with AMS PMF	Urban backg. Rural backg. Biomass burning	 *15.4*	1.7 4
Huang et al. 2013	AMS PMF for POA, SP2 for BC	Urban backg. winter Urban backg. summer	**0.82** **1.27**	
Hayes et al. 2013	AMS PMF for POA, SP2 for BC	Urban background	**1.82** (average) 1.51 (more diesel influenced)	
Crippa et al. 2013	AMS PMF for POA, Aethalometer for BC	Urban mobile sources Cooking aerosol Residential burning	**0.5 (ave)** **0.5 (ave)** 3.4 (ave)	
Huang et al. 2015	Offline AMS and TOT OC/EC analyzer, ME2 analysis	Traffic Cooking	**0.5** **2.5**	

		BB	11	
Zhang et al. 2015	14C source apportionment for EC and OC	Fossil fuel, coal burning Residential burning		1.6 *8.5*
Hu et al. 2016	AMS PMF for POA, SP2 for BC	Urban Background	**1.4**	
Kim et al. 2018	AMS PMF for POA, SP2 for BC	Urban background (70% HOA, 30% COA)	**2.2**	
Whatore et al. 2017	TOT EC/OC analyzer	African traditional stoves		*4.8*
Nault et al. 2018	AMS PMF for POA, SP2 for BC	Urban background	**2.38**	
Chen et al. 2018	AMS PMF for POA, SP2 for BC	BB urban BB rural	*6.25* *5*	
Chirico et al. 2011	AMS OA SP2 for BC	Tunnel mobile emissions	0.4	
Kim et al. 2017	AMS PMF for POA, SP2 for BC	Total urban POA (40% BB, 27% HOA, 33% COA)	3.2	
Andreae, 2019	Review (OA/OC of 1.6 used per the methodology of the review)	Savanna Tropical forest b Temperate forest b Boreal forest b Peat AG Dung Biofuel Charcoal Average (used in this work)		*9.1* *13.8* *31.7* *22* *227* *18.7* *9.9* *52.6* *13* ***11.8***

155

156

157

Table S2: POA/BC ratios as derived from several emission inventories and as found in published ambient measurements.

Source	Type of emissions	POA/BC ratio (POA=1.4*POC)	POA/BC ratio (POA=1.8*POC)	Emission year
NEI Reff et al. (2009)	Heavy duty diesel vehicles	0.3	0.4	2001
	Light duty diesel vehicles	1.0	1.2	
	Nonroad gasoline exhaust	5.4	7.0	
	Onroad gasoline exhaust	5.2	4.0	
	Residential wood comb.	13.2	17.0	
	Residential coal combustion	2.6	3.4	
	Residential natural gas comb.	10.2	13.2	
Biomass burning Akagi et al. (2011)	Tropical Forest	11.0	14.2	N/A
	Savanna	9.9	12.7	
	Crop Residue	4.3	5.5	
	Pasture Maintenance	14.8	19.1	
	Extratropical Forest	22.9	29.4	
	Peatland	43.6	56.1	
	Chaparral	4.0	5.1	
	Open Cooking	4.9	6.3	
	Stoves	3.6	4.7	
	Charcoal Making	51.8	66.6	
	Charcoal Burning	1.8	2.3	
	Dung Burning	4.8	6.1	
	Garbage Burning	11.4	14.6	
Bond et al. (2004)	Total Fossil fuel	1.1	1.4	1996
	Total Biofuel/Biomass	8.7	11.2	
	Open burning/forest	12.7	16.3	
	Open burning/savanna	9.9	12.7	
	Open burning/crop residue	6.7	8.6	
	Coal/power generation	1.0	1.3	
	Diesel fuel/on-road	0.5	0.7	
	Wood/residential	5.6	7.2	
	Agricultural waste/residential	5.3	6.8	
	Animal waste/residential	5.0	6.5	
	Coal/industry	1.0	1.3	
	Diesel fuel/residential	0.5	0.6	
	Coal/residential	1.2	1.6	
	Diesel fuel/off-road	0.7	0.9	
	Gasoline/transport	10.1	13.0	
	Other combustion	2.3	2.9	
CEDS inventory (CMIP 6)	Energy	2.4	3.1	2014
	Transportation	0.6	0.8	
	Ships	1.1	1.4	
	Residential	4.2	5.4	
	Industrial process	2.5	3.2	
	Waste	8.7	11.2	
	Total	3.4	4.4	

ACCLIP	Energy	9.6	12.3	2000
	Transportation	1.5	1.9	
	Industries	2.1	2.7	
	Residential	5.6	7.2	
	Agricultural waste	6.7	8.6	
	Waste	1.9	2.4	
	Total	3.5	4.5	
EDGAR v4.3.2	Aviation climbing and descent	0.7	0.9	2012
	Aviation cruise	0.7	0.9	
	Aviation landing and take off	0.7	0.9	
	Oil refineries and transformation	0.2	0.3	
	Energy industry	1.6	2.1	
	Combustion in manufacturing industry	2.7	3.4	
	Fuel exploitation	0.1	0.2	
	Non-road ground transportation	1.5	1.9	
	Ships	0.7	0.9	
	Road transportation	1.1	1.4	
	Residential and other sectors	5.4	6.9	
	Agricultural waste burning	21.0	27.0	
	Waste incineration	2.4	3.1	
	Fossil Fuel fires	0.7	0.9	
	Total	3.5	4.5	

160

161

Table S3: Similar to table 2 but for sulfate aerosols. The statistical indicators are calculated as normalized mean bias $NMB(\%) = 100 \times \sum_i (M_i - O_i) / \sum_i O_i$; normalized mean error $NME(\%) = 100 \times \sum_i |(M_i - O_i)| / \sum_i O_i$; root mean square error $RMSE(\mu g\, m^{-3}) = \sqrt{(1/N) \sum_i (M_i - O_i)^2}$ and correlation coefficient (R^2) between modeled (M_i) and observed (O_i) data points. The mean of ATom-1 sulfate observations is ~0.18 μg m^{-3} and for ATom-2 is ~0.165 μg m^{-3}.

Sulfate	Avg.Mod. (μg m^{-3})	NMB (%)	NME (%)	RMSE (μg m^{-3})	R^2	Avg.Mod. (μg m^{-3})	NMB (%)	NME (%)	RMSE (μg m^{-3})	R^2
Model	*ATom-1 scores (August 2016)*					*ATom-2 scores (February 2017)*				
ATom Ensemble	0.188	-0.31	73.8	0.446	0.21	0.163	-3.3	65.2	0.234	0.20
CESM2-DYN	0.197	2.3	86.0	0.471	0.16	0.113	-33.6	65.2	0.322	0.15
CESM2-SMP	0.190	-1.1	85.3	0.475	0.15	0.106	-38.0	64.1	0.306	0.23
CESM1-CARMA	0.161	-11.0	89.4	0.455	0.12	0.106	-36.4	72.9	0.420	0.05
ECHAM6-HAM	0.518	190	263	0.785	0.03	0.471	191.5	262.8	0.634	0.01
GC12-DYN	0.205	13.4	79.6	0.413	0.24	0.216	21.0	82.5	0.251	0.15
GC12-REF	0.211	16.9	80.9	0.414	0.24	0.222	24.4	79.5	0.245	0.17
GC10-TOMAS	0.202	8.2	85.6	0.445	0.15	0.211	25.9	91.1	0.289	0.04
GEOS5	0.110	-43.2	69.1	0.468	0.11	0.103	-40.6	71.9	0.237	0.10

References:

Aiken, a. C., Salcedo, D., Cubison, M. J., Huffman, J. a., DeCarlo, P. F., Ulbrich, I. M., Docherty, K. S., Sueper, D., Kimmel, J. R., Worsnop, D. R., Trimborn, A., Northway, M., Stone, E. a., Schauer, J. J., Volkamer, R. M., Fortner, E., de Foy, B., Wang, J., Laskin, A., Shutthanandan, V., Zheng, J., Zhang, R., Gaffney, J., Marley, N. a., Paredes-Miranda, G., Arnott, W. P., Molina, L. T., Sosa, G. and Jimenez, J. L.: Mexico City aerosol analysis during MILAGRO using high resolution aerosol mass spectrometry at the urban supersite (T0) – Part 1: Fine particle composition and organic source apportionment, Atmos. Chem. Phys., 9(17), 6633–6653, doi:10.5194/acp-9-6633-2009, 2009.

Andreae, M. O.: Emission of trace gases and aerosols from biomass burning – an updated assessment, Atmos. Chem. Phys., 19(13), 8523–8546, doi:10.5194/acp-19-8523-2019, 2019.

Ban-Weiss, G. A., McLaughlin, J. P., Harley, R. A., Lunden, M. M., Kirchstetter, T. W., Kean, A. J., Strawa, A. W., Stevenson, E. D. and Kendall, G. R.: Long-term changes in emissions of nitrogen oxides and particulate matter from on-road gasoline and diesel vehicles, Atmos. Environ., 42(2), 220–232, doi:10.1016/j.atmosenv.2007.09.049, 2008.

Chen, C. L., Chen, S., Russell, L. M., Liu, J., Price, D. J., Betha, R., Sanchez, K. J., Lee, A. K. Y., Williams, L., Collier, S. C., Zhang, Q., Kumar, A., Kleeman, M. J., Zhang, X. and Cappa, C. D.: Organic Aerosol Particle Chemical Properties Associated With Residential Burning and Fog in Wintertime San Joaquin Valley (Fresno) and With Vehicle and Firework Emissions in Summertime South Coast Air Basin (Fontana), J. Geophys. Res. Atmos., 123(18), 10,707-10,731, doi:10.1029/2018JD028374, 2018.

Chirico, R., DeCarlo, P. F., Heringa, M. F., Tritscher, T., Richter, R., Prévôt, A. S. H., Dommen, J., Weingartner, E., Wehrle, G., Gysel, M., Laborde, M. and Baltensperger, U.: Impact of aftertreatment devices on primary emissions and secondary organic aerosol formation potential from in-use diesel vehicles: results from smog chamber experiments, Atmos. Chem. Phys., 10(23), 11545–11563, doi:10.5194/acp-10-11545-2010, 2010.

Chirico, R., Prevot, A. S. H., DeCarlo, P. F., Heringa, M. F., Richter, R., Weingartner, E. and Baltensperger, U.: Aerosol and trace gas vehicle emission factors measured in a tunnel using an Aerosol Mass Spectrometer and other on-line instrumentation, Atmos. Environ., 45(13), 2182–2192, doi:10.1016/j.atmosenv.2011.01.069, 2011.

Christian, T. J., Yokelson, R. J., Cárdenas, B., Molina, L. T., Engling, G. and Hsu, S.-C.: Trace gas and particle emissions from domestic and industrial biofuel use and garbage

burning in central Mexico, Atmos. Chem. Phys., 10(2), 565–584, doi:10.5194/acp-10-565-2010, 2010.

Crippa, M., Canonaco, F., Slowik, J. G., El Haddad, I., DeCarlo, P. F., Mohr, C., Heringa, M. F., Chirico, R., Marchand, N., Temime-Roussel, B., Abidi, E., Poulain, L., Wiedensohler, a., Baltensperger, U. and Prévôt, a. S. H.: Primary and secondary organic aerosol origin by combined gas-particle phase source apportionment, Atmos. Chem. Phys., 13(16), 8411–8426, doi:10.5194/acp-13-8411-2013, 2013.

Goetz, J. D., Giordano, M. R., Stockwell, C. E., Christian, T. J., Maharjan, R., Adhikari, S., Bhave, P. V, Praveen, P. S., Panday, A. K., Jayarathne, T., Stone, E. A., Yokelson, R. J. and DeCarlo, P. F.: Speciated online PM1 from South Asian combustion sources – Part 1: Fuel-based emission factors and size distributions, Atmos. Chem. Phys., 18(19), 14653–14679, doi:10.5194/acp-18-14653-2018, 2018.

Haslett, S. L., Thomas, J. C., Morgan, W. T., Hadden, R., Liu, D., Allan, J. D., Williams, P. I., Keita, S., Liousse, C. and Coe, H.: Highly controlled, reproducible measurements of aerosol emissions from combustion of a common African biofuel source, Atmos. Chem. Phys., 18(1), 385–403, doi:10.5194/acp-18-385-2018, 2018.

Hayes, P. L., Ortega, A. M., Cubison, M. J., Froyd, K. D., Zhao, Y., Cliff, S. S., Hu, W. W., Toohey, D. W., Flynn, J. H., Lefer, B. L., Grossberg, N., Alvarez, S., Rappenglück, B., Taylor, J. W., Allan, J. D., Holloway, J. S., Gilman, J. B., Kuster, W. C., de Gouw, J. A., Massoli, P., Zhang, X., Liu, J., Weber, R. J., Corrigan, A. L., Russell, L. M., Isaacman, G., Worton, D. R., Kreisberg, N. M., Goldstein, A. H., Thalman, R., Waxman, E. M., Volkamer, R., Lin, Y. H., Surratt, J. D., Kleindienst, T. E., Offenberg, J. H., Dusanter, S., Griffith, S., Stevens, P. S., Brioude, J., Angevine, W. M. and Jimenez, J. L.: Organic aerosol composition and sources in Pasadena, California, during the 2010 CalNex campaign, J. Geophys. Res. Atmos., 118(16), 9233–9257, doi:10.1002/jgrd.50530, 2013.

Huang, R. J., Zhang, Y., Bozzetti, C., Ho, K. F., Cao, J. J., Han, Y., Daellenbach, K. R., Slowik, J. G., Platt, S. M., Canonaco, F., Zotter, P., Wolf, R., Pieber, S. M., Bruns, E. A., Crippa, M., Ciarelli, G., Piazzalunga, A., Schwikowski, M., Abbaszade, G., Schnelle-Kreis, J., Zimmermann, R., An, Z., Szidat, S., Baltensperger, U., El Haddad, I. and Prévôt, A. S. H.: High secondary aerosol contribution to particulate pollution during haze events in China, Nature, 514(7521), 218–222, doi:10.1038/nature13774, 2015.

Huang, X. F., Xue, L., Tian, X. D., Shao, W. W., Sun, T. Le, Gong, Z. H., Ju, W. W., Jiang, B., Hu, M. and He, L. Y.: Highly time-resolved carbonaceous aerosol characterization in

Yangtze River Delta of China: Composition, mixing state and secondary formation, Atmos. Environ., 64, 200–207, doi:10.1016/j.atmosenv.2012.09.059, 2013.

Kim, H., Zhang, Q. and Heo, J.: Influence of intense secondary aerosol formation and long-range transport on aerosol chemistry and properties in the Seoul Metropolitan Area during spring time: Results from KORUS-AQ, Atmos. Chem. Phys., 18(10), 7149–7168, doi:10.5194/acp-18-7149-2018, 2018.

Kim, H., Zhang, Q., Bae, G.-N., Kim, J. Y. and Lee, S. B.: Sources and atmospheric processing of winter aerosols in Seoul, Korea: insights from real-time measurements using a high-resolution aerosol mass spectrometer, Atmos. Chem. Phys., 17(3), 2009–2033, doi:10.5194/acp-17-2009-2017, 2017.

Minguillon, M. C., Perron, N., Querol, X., Szidat, S., Fahrni, S. M. M., Alastuey, A., Jimenez, J. L. L., Mohr, C., Ortega, A. M. M., Day, D. A. A., Lanz, V. A. A., Wacker, L., Reche, C., Cusack, M., Amato, F., Kiss, G., Hoffer, A., Decesari, S., Moretti, F., Hillamo, R., Teinila, K., Seco, R., Penuelas, J., Metzger, A., Schallhart, S., Muller, M., Hansel, A., Burkhart, J. F. F., Baltensperger, U., Prevot, A. S. H., Minguillón, M. C., Perron, N., Querol, X., Szidat, S., Fahrni, S. M. M., Alastuey, A., Jimenez, J. L. L., Mohr, C., Ortega, A. M. M., Day, D. A. A., Lanz, V. A. A., Wacker, L., Reche, C., Cusack, M., Amato, F., Kiss, G., Hoffer, A., Decesari, S., Moretti, F., Hillamo, R., Teinilä, K., Seco, R., Peñuelas, J., Metzger, A., Schallhart, S., Müller, M., Hansel, A., Burkhart, J. F. F., Baltensperger, U. and Prévót, A. S. H.: Fossil versus contemporary sources of fine elemental and organic carbonaceous particulate matter during the DAURE campaign in Northeast Spain, Atmos. Chem. Phys., 11(23), 12067–12084, doi:doi:10.5194/acp-11-12067-2011, 2011.

Nault, B. A., Campuzano-Jost, P., Day, D. A., Schroder, J. C., Anderson, B., Beyersdorf, A. J., Blake, D. R., Brune, W. H., Choi, Y., Corr, C. A., de Gouw, J. A., Dibb, J., DiGangi, J. P., Diskin, G. S., Fried, A., Huey, L. G., Kim, M. J., Knote, C. J., Lamb, K. D., Lee, T., Park, T., Pusede, S. E., Scheuer, E., Thornhill, K. L., Woo, J.-H. and Jimenez, J. L.: Secondary organic aerosol production from local emissions dominates the organic aerosol budget over Seoul, South Korea, during KORUS-AQ, Atmos. Chem. Phys., 18(24), 17769–17800, doi:10.5194/acp-18-17769-2018, 2018.

Reddington, C. L., Yoshioka, M., Balasubramanian, R., Ridley, D., Toh, Y. Y., Arnold, S. R. and Spracklen, D. V.: Contribution of vegetation and peat fires to particulate air pollution in Southeast Asia, Environ. Res. Lett., 9(9), doi:10.1088/1748-9326/9/9/094006, 2014.

289 Reff, A., Bhave, P. V., Simon, H., Pace, T. G., Pouliot, G. A., Mobley J. D., Houyoux, M.:
290 Emissions Inventory of PM2.5 Trace Elements across the United States, Environ. Sci.
291 Technol. 43, 15, 5790-5796, 2009.
292
293 Shen, G., Wei, S., Wei, W., Zhang, Y., Min, Y., Wang, B., Wang, R., Li, W., Shen, H.,
294 Huang, Y., Yang, Y., Wang, W., Wang, X., Wang, X. and Tao, S.: Emission factors, size
295 distributions, and emission inventories of carbonaceous particulate matter from residential
296 wood combustion in rural china, Environ. Sci. Technol., 46(7), 4207–4214,
297 doi:10.1021/es203957u, 2012.
298
299 Shen, G., Xue, M., Chen, Y., Yang, C., Li, W., Shen, H., Huang, Y., Zhang, Y., Chen, H.,
300 Zhu, Y., Wu, H., Ding, A. and Tao, S.: Comparison of carbonaceous particulate matter
301 emission factors among different solid fuels burned in residential stoves, Atmos. Environ.,
302 89, 337–345, doi:10.1016/j.atmosenv.2014.01.033, 2014.
303
304 Szidat, S., Jenk, T. M., Synal, H. A., Kalberer, M., Wacker, L., Hajdas, I., Kasper-Giebl,
305 A. and Baltensperger, U.: Contributions of fossil fuel, biomass-burning, and biogenic
306 emissions to carbonaceous aerosols in Zurich as traced by 14C, J. Geophys. Res. Atmos.,
307 111(7), 1–12, doi:10.1029/2005JD006590, 2006.
308
309 Wathore, R., Mortimer, K. and Grieshop, A. P.: In-Use Emissions and Estimated Impacts
310 of Traditional, Natural- and Forced-Draft Cookstoves in Rural Malawi, Environ. Sci.
311 Technol., 51(3), 1929–1938, doi:10.1021/acs.est.6b05557, 2017.
312
313 Zhang, Y.-L., Huang, R.-J., El Haddad, I., Ho, K.-F., Cao, J.-J., Han, Y., Zotter, P.,
314 Bozzetti, C., Daellenbach, K. R., Canonaco, F., Slowik, J. G., Salazar, G., Schwikowski,
315 M., Schnelle-Kreis, J., Abbaszade, G., Zimmermann, R., Baltensperger, U., Prévôt, A. S.
316 H. and Szidat, S.: Fossil vs. non-fossil sources of fine carbonaceous aerosols in four
317 Chinese cities during the extreme winter haze episode of 2013, Atmos. Chem. Phys., 15(3),
318 1299–1312, doi:10.5194/acp-15-1299-2015, 2015.